Performance Analysis of a 30 kW Dynamic Wireless Power Transfer System for Electric Vehicle

Yao Pei, Karim Kadem, Lionel Pichon, Mohamed Bensetti, Yann Le Bihan

Performance Analysis of a 30 kW Dynamic Wireless Power Transfer System for Electric Vehicle

Yao Pei
Université Paris-Saclay, CentraleSupélec, CNRS, Laboratoire de Génie Electrique et Electronique de Paris, 91192, Gif-sur-Yvette, France
Sorbonne Université, CNRS, Laboratoire de Génie Electrique et Electronique de Paris, 75252, Paris, France
yao.pei@centralesupelec.fr

Karim Kadem
Institut VEDECOM, 23 bis Allée des Marronniers, 78000 Versailles, France
karim.kadem@vedecom.fr

Lionel Pichon
Université Paris-Saclay, CentraleSupélec, CNRS, Laboratoire de Génie Electrique et Electronique de Paris, 91192, Gif-sur-Yvette, France
Sorbonne Université, CNRS, Laboratoire de Génie Electrique et Electronique de Paris, 75252, Paris, France
lionel.pichon@centralesupelec.fr

Mohamed Bensetti
Université Paris-Saclay, CentraleSupélec, CNRS, Laboratoire de Génie Electrique et Electronique de Paris, 91192, Gif-sur-Yvette, France
Sorbonne Université, CNRS, Laboratoire de Génie Electrique et Electronique de Paris, 75252, Paris, France
mohamed.bensetti@centralesupelec.fr

Yann Le Bihan
Université Paris-Saclay, CentraleSupélec, CNRS, Laboratoire de Génie Electrique et Electronique de Paris, 91192, Gif-sur-Yvette, France
Sorbonne Université, CNRS, Laboratoire de Génie Electrique et Electronique de Paris, 75252, Paris, France
yann.le-bihan@geeps.centralesupelec.fr

***Abstract*—The present work aims at quantifying how the position of the receiver in a realistic dynamic wireless power transfer (DWPT) system affects the transmission process for electric vehicles. With the aim of considering the transmitted power, the position of the receiver is influenced by the factors that are the moving distance along the X axis, the misalignment along the Y axis, the vertical variation along the Z axis and the rotation angle along the Z axis. The analysis is based on the polynomial chaos expansions for a low computational cost and a fast sensitivity analysis.**

Keywords—dynamic wireless power transfer system, FEM modeling, metamodeling, performance analysis

I. INTRODUCTION

The electrification of transportation means has taken importance in recent years, especially in the automotive domain, where the problems of global warming are driving manufacturers to find cleaner solutions that are more respectful of the environment. However, energy storage is always the main drawback of Electric Vehicles (EVs). EVs cannot travel across too much distance with the limited electricity of the battery [1-4]. So the use of dynamic wireless power transfer (DWPT) charging systems could be the most promising solution to solve the range anxiety: the vehicle is charged while driving [1-2]. This type of charging has the advantage of being transparent to the user and ergonomic, allowing simultaneous charging and use of the vehicle. So the capacity of energy storage can be largely reduced, and the driving range is extended when the DWPT charging system is employed [3].

However, the design of a DWPT system involves system-level specifications that must be matched with a proper choice of architectures and components. These requirements include system performances (efficiency, voltage, current, magnetic leakage), budgets (cost, volume), environmental conditions, and system reliability (robustness, lifetime). So, 3D computations are needed to assess the performance of the DWPT system. Nevertheless, the use of complex simulation tools leads to heavy computations in case of wide parametric analysis. In this case, the standard Monte Carlo (MC) analysis is becoming challenging in terms of computer resources and simulation time. So, several metamodeling techniques have been developed, such as Support Vector Regression (SVR), Multigene Genetic Programming Algorithm (MGPA), Polynomial Chaos Expansions (PCE), and so on. For example, reference [5] concludes, thanks to polynomial chaos expansions metamodels, that the circular shape of the coupling coils is the best for static inductive power transfer system, while reference [6] introduces that the square shape is the best for DWPT systems considering the coupling coefficient with the variation of the misalignment. Then, some research papers [7-9] showed how the uncertainties on the components and material parameters of a wireless power transfer system for the static charge of electric vehicles affect the overall efficiency based on several metamodeling techniques. However, they did not analyze the power transmission for DWPT systems.

The main contribution of the work consists of an accurate analysis to determine how the performance of a realistic DWPT system (built by VEDECOM), including the power transmission and the magnetic flux density leakage, can be affected by the position of the receiver. This type of analysis is of great interest, especially in view of real system implementation and an industrial design process. The adoption of Polynomial Chaos Expansions (PCE) as a metamodel allows for performing the analysis in a very efficient way and with a computational cost significantly reduced with respect to conventional simulation techniques. To the best of the authors' knowledge, such PCE metamodel analysis based on realistic DWPT systems has not been presented in the literature yet.

The rest of the paper is organized as follows. Section II provides a general description of DWPT systems for EVs and proposes a realistic 3D model of the magnetic coupler connected with series-series electric circuits. Section III presents an overview of the sparse PCE metamodel and the

sensitivity analysis based on it. In Section IV, the considered influencing factors and their characteristics are described, and how they influence the transmitted power, the current ratio and the magnetic flux density leakage is analyzed with the sparse PCE metamodel. Finally, in Section V, the main outcomes of the work are summarized.

II. DYNAMIC WIRELESS POWER TRANSFER SYSTEM

Fig.1 shows a DWPT system characterization bench, which has been designed and built in VEDECOM [10]. The magnetic coupler consists of an active transmitter (primary coil + ferrite plate). This transmitter is integrated into the ground (road) and carries an alternating current, creating an alternating magnetic field that generates an AC voltage across the receiver (secondary coil + ferrite plate) on the EVs. The two coils of the coupler are placed near ferrite plates to channel the magnetic field. All the system is located under a shielding (aluminum plate) as a screen. The operating parameters of the system considered in this paper are listed in Table I.

For the DWPT system transmission efficiency, circuit models with lumped parameters are often used. Compensation networks are designed to minimize the reactive power, make the system high misalignment tolerant, and achieve high efficiency. Here, the series-series (SS) compensation is taken into account for the reason that it provides good efficiency and the capacitance values don't depend on the load variation, which is very useful in DWPT systems [3-4].

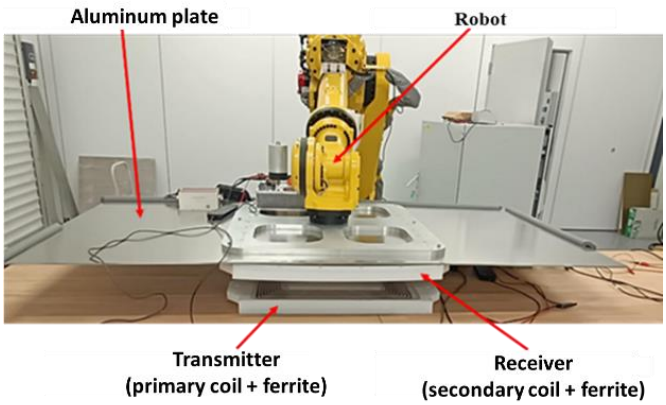

Fig. 1. Dynamic Wireless Power Transfer System in VEDECOM

TABLE I. PARAMETERS AND DWPT OPERATING STATUS

Parameter	Value	Unit
Resonant frequency f_0	85	kHz
Transmitter power	30	kW
Transmitting coil current (RMS Value)	17	A
Air gap	150-180	mm
Load R_L	5.3	Ω

In Fig.2, the transmitter resistance R_1, the receiver resistance R_2, the transmitter self-inductance L_1, the receiver self-inductance L_2 and the mutual inductance M between the transmitter and the receiver in the red dotted box represents the electrical parameters of the magnetic coupler, which is below the electric circuits. Through the analysis, the output power P_2 in the load and the ratio A_I between the output current I_1 and the input current I_2 can be described [11]:

$$P_2 = real(V_L \times I_2^*) \quad (1)$$

$$A_I = \frac{I_2}{I_1} = |A_1| e^{j\theta_1} \quad (2)$$

where V_L is the voltage on the load, and I_2^* represents the conjugate of the output current I_2. Normally, the phase difference θ_1 between the input and the output for the current is almost 90° at the resonant frequency [11].

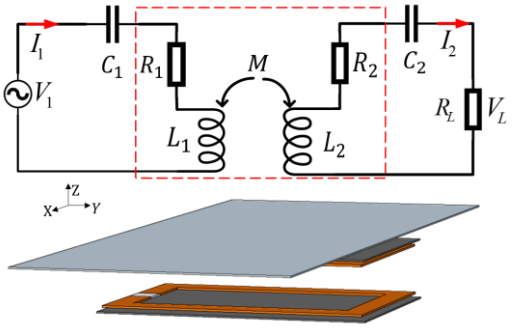

Fig. 2. SS compensation for DWPT system

As shown in Fig.3, the magnetic coupler is a realistic 3D structure consisting of two identical rectangle-shaped coils with copper windings (orange), ferrite core plates (dark grey), and an aluminum plate (blue). The dimensions of the magnetic coupler are shown in Table II. The size of the aluminum plate depends on the sizes of the coils and of the ferrite plates [12]. Furthermore, according to the ICNIRP guidelines and SAE J2954 standard [13-14], the magnetic flux density leakage B_{leak} at the observation point which is 800 mm far from the center of the air gap should be smaller than 27 μT (RMS value), also as shown in Fig. 3.

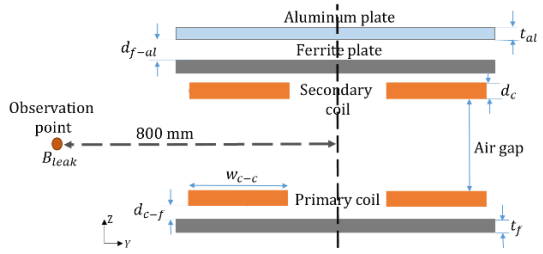

(a)

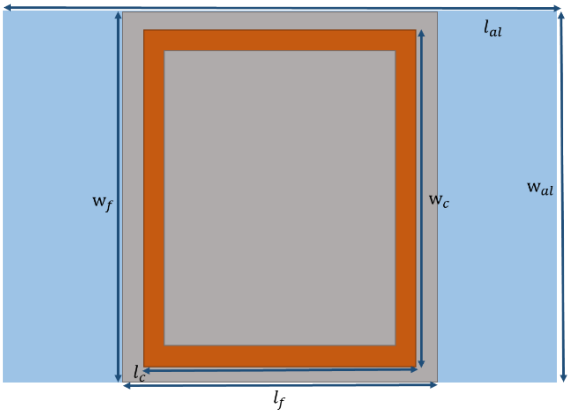

(b)

Fig. 3. (a) A pair of coils (orange) with ferrite plate (grey) and aluminum plate (blue) and (b) a single rectangular coil with ferrite and aluminum plate

TABLE II. PARAMETERS OF THE DWPT SYSTEM

Symbol	Quantity	Value [Unit]
l_c	External length dimension of the coils	570 [mm]
w_c	External width dimension of the coils	970 [mm]
d_c	Coil thickness	7 [mm]
w_{c-c}	Coil width	84 [mm]
l_f	Ferrite length	600 [mm]
w_f	Ferrite width	1000 [mm]
d_{c-f}	Distance between coil and ferrite	13 [mm]
t_f	Ferrite thickness	5 [mm]
l_{al}	Aluminum plate length	2000 [mm]
w_{al}	Aluminum plate width	1000 [mm]
t_{al}	Aluminum plate thickness	5 [mm]
d_{f-al}	Distance between ferrite and Aluminum plate	14.7 [mm]
μ_r	Ferrite relative permeability	3000
σ_{sh}	Aluminum plate conductivity	34.2 [MS/m]
N	Coil turns	8

However, in a real scenario for the DWPT systems, various positions of the receiver may happen during the charging process. So it is meaningful to observe how the output power P_2, the current amplitude ratio $|A_I|$, the current phase difference θ_I between the input and the output, and the magnetic flux density leakage B_{leak} of the obseved point vary with different positions of the receiver. Such investigations can be performed with standard 3D software modeling tools, but they lead to a computational burden in case of parameteric sweeps. Then, in order to save the computational time, a metamodel based on polynomial chaos expansions provides a fast analysis with a reduced number of calculations by COMSOL 3D finite element software. Moreover, a suitable sensitivity analysis can be obtained on this metamodel.

III. POLYNOMIAL CHAOS EXPANSIONS

Polynomial Chaos Expansions (PCE) metamodeling is a powerful metamodeling technique that aims at analyzing the relationship between the input parameters and the outputs in a non-intrusive way and help find the most influential input parameter to the output in high-dimensional problems. The results given in this paper were obtained by means of the UQLAB toolbox [15].

It starts by considering the vector $\boldsymbol{x} \in \mathbb{R}^d$ collecting d independent input parameters $\boldsymbol{x} = \{x_1, \cdots, x_d\}$ with a joint probability density function (PDF) $f_{\mathbf{x}}(\boldsymbol{x})$. $\boldsymbol{x}$ represents the influencing factors (the moving distance along the X axis, the misalignment along the Y axis, the vertical variation along the Z axis and the rotation angle along the Z axis, which will be described detailedly in Section IV) that decides the position of the receiver. Assuming that the problem is described by the corresponding outputs $\boldsymbol{y} = \{y_1, \cdots, y_N\}$, the PCE metamodel is established to evaluate the varying trend of the outputs (the output power P_2, the current amplitude ratio $|A_I|$ and the current phase difference θ_I between the input current and the output current separately, and the magnetic flux density leakage B_{leak}) [8-9, 15-17]:

$$M^{PCE}(\boldsymbol{x}) = \sum_{\alpha \in \mathbb{N}^d} \hat{c}_\alpha \Phi_\alpha(\boldsymbol{x}) \quad (3)$$

where $\Phi_\alpha(\boldsymbol{x})$ are multivariate polynomials basis functions with the corresponding coefficients $\hat{c}_\alpha$. $\alpha \in \mathbb{N}^d$ is a multi-index that identifies the components of the multivariate polynomials Φ_α.

In this section, the coefficients $\hat{c}_\alpha$ are estimated by using a non-intrusive technique: the Least Angle Regression (LAR) [16] from a set of the outputs $\boldsymbol{y}$. This technique relies on the choice of a truncation set denoted $\mathcal{A} = \{\alpha_0, \cdots, \alpha_{p-1}\} \subset \mathbb{N}^d$ defining the multi-indices of the selected basis polynomials $\{\Phi_{\alpha_0}, \cdots, \Phi_{\alpha_{p-1}}\}$. In order to decrease the size of PCE coefficients when dealing with high-dimensional problems, the hyperbolic truncation strategy $\mathcal{A}_q^{d,p}$ based on the total degree p and a parameter q, with $0 < q < 1$, allowing for reducing the size of the PCE basis is then defined as follows [15-18]:

$$\mathcal{A}_q^{d,p} = \left\{\alpha \in \mathbb{N}^d : \|\alpha\|_q = \left(\sum_{i=1}^d \alpha_i^q\right)^{\frac{1}{q}} \leq p\right\} \quad (4)$$

The way to estimate the accuracy of PCE metamodel can be: leave-one-out (LOO) error ϵ_{LOO}. It is designed to overcome the over-fitting limitation by using cross-validation, a technique developed in statistical learning theory. It consists in building N separate PCE metamodels $M^{PCE\backslash i}$, each one created on reduced model evaluations $\boldsymbol{x}\backslash\boldsymbol{x}^{(i)} = \{\boldsymbol{x}^{(j)}, j = 1, \cdots, N, j \neq i\}$ and comparing its prediction on the excluded point $\boldsymbol{x}^{(i)}$ with the real value $\boldsymbol{y}(\boldsymbol{x}^{(i)})$. It can be written as [13-15]:

$$\epsilon_{LOO} = \frac{\sum_{i=1}^N (\boldsymbol{y}(\boldsymbol{x}^{(i)}) - M^{PCE\backslash i}(\boldsymbol{x}^{(i)}))^2}{\sum_{i=1}^N (\boldsymbol{y}(\boldsymbol{x}^{(i)}) - \overline{\boldsymbol{y}(\boldsymbol{x})})^2} \quad (5)$$

Expect the training data set used to construct the PCE metamodel, an additional set of the input parameters and the outputs, called the test data set, $D_{test} = \{\left(\boldsymbol{x}_{test}^{(i)}, \boldsymbol{y}\left(\boldsymbol{x}_{test}^{(i)}\right)\right), i = 1, \cdots, N_{test}\}$ is available, and the test error can be calculated as [16]:

$$\epsilon_{test} = \frac{N_{test}-1}{N_{test}} \left[\frac{\sum_{i=1}^{N_{test}} (\boldsymbol{y}\left(\boldsymbol{x}_{test}^{(i)}\right) - M^{PCE}(\boldsymbol{x}_{test}^{(i)}))^2}{\sum_{i=1}^{N_{test}} (\boldsymbol{y}\left(\boldsymbol{x}_{test}^{(i)}\right) - \hat{\mu}_{test})^2}\right] \quad (6)$$

where $\hat{\mu}_{test} = \frac{1}{N_{test}} \sum_{i=1}^{N_{test}} \boldsymbol{y}\left(\boldsymbol{x}_{test}^{(i)}\right)$ is the mean of the test data set responses and $M^{PCE}(\boldsymbol{x}_{test}^{(i)})$ is the prediction value based on the PCE metamodel.

Then, in order to identify quantities of interest in the model response, a post-processing of the coefficients of PCE metamodel can be performed at a relatively low computational cost. The mean value is the first coefficient of the PCE metamodel, and the variance is computed as the sum of the squares of the remaining coefficients [15-16].

$$\text{Mean value: } \hat{\mu}_{\boldsymbol{y}} = \mathbb{E}[\boldsymbol{y}] = \hat{c}_0 \quad (7)$$

$$\text{Variance: } \hat{\sigma}_{\boldsymbol{y}}^2 = \mathbb{V}[M^{PCE}(\boldsymbol{x})] = \sum_{\alpha \epsilon A \backslash \{0\}} \hat{c}_\alpha^2 \quad (8)$$

After, the global sensitivity analysis aims at quantifying which input parameter(s) $\boldsymbol{x}$ influence the outputs $\boldsymbol{y}$ variability most. It can be calculated by the PCE coefficients. The first-order PCE-based Sobol index S_i of the outputs $\boldsymbol{y}$ quantifies the additive effect of each input parameter separately [19-20]:

$$S_i = \frac{D_i}{D} = \frac{\mathbb{V}_{x_i}(\mathbb{E}_{x_{\sim i}}(M^{PCE}(\boldsymbol{x})|x_i))}{\mathbb{V}[M^{PCE}(\boldsymbol{x})]} = \frac{\sum_{\alpha \epsilon \mathcal{A}_i} \hat{c}_\alpha^2}{\sum_{\alpha \epsilon \mathcal{A} \backslash \{0\}} \hat{c}_\alpha^2} \quad (9)$$

with $\mathcal{A}_i = \{\alpha \in \mathcal{A}: \alpha_i > 0, \alpha_j = 0\ \forall j \neq i\}$ and $x_{\sim i}$ notation indicates the set of all variables except x_i. The first-order PC-based Sobol index of the i^{th} variable is closer to 1 means that the i^{th} variable has more impact on the outputs $\boldsymbol{\mathcal{Y}}$.

IV. Results and Discussions

To investigate the performance of the DWPT system, it is mandatory to take into account the position of the receiver. So the influencing factors are the variations in the misalignment during the driving and variations in the air gap due to loading or unloading the vehicle. Fig.4 shows the rotation angle α along the Z axis, the moving distance ΔX along the X axis (respresents the direction of EV movement), the misalignment ΔY along the Y axis , and the vertical variation ΔZ along the Z axis.

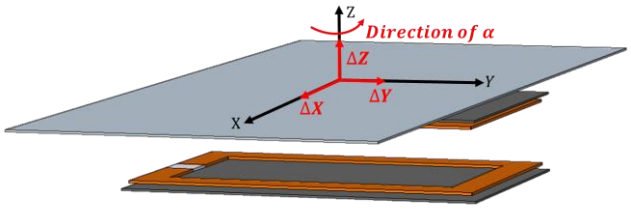

Fig. 4. Influencing factors on the receiver

TABLE III. Properties of the Influencing Factors

Influencing factors	Symbol	Probability Density Distribution	Mean Value	Standard Deviation
Misalignment along Y axis [mm]	ΔY	Gaussian	0	162
Vertical variation along Z axis [mm]	ΔZ	Gaussian	165	5
Rotation angle along Z axis [deg]	α	Gaussian	0	10
Influencing factors	**Symbol**	**Probability Density Distribution**	**Min Value**	**Max Value**
Moving distance along X axis [mm]	$\Delta \boldsymbol{X}$	Uniform	0	285

The sparse PCE metamodel has been adopted to quantify the impact of these influencing factors on this DWPT system (including the output power P_2, the current amplitude ratio A_I, the current phase difference θ_I between the input and the output, and the magnetic flux density leakage B_{leak}). In addition, the sparse PCE metamodels are constructed with an adaptive degree varying from 3 to 15, and the hyperbolic scheme in Equation (4) is set to $q = 0.75$ to reduce the size of the polynomial basis [15-16].

All of the sparse PCE metamodels have been trained from a training data set containing 387 training samples selected by Latin Hypercube Sampling (LHS) [21] resulting from COMSOL calculations with a computational cost of 8.5 h (one calculation in the COMOSL 3D model takes about 78 s). In order to investigate the performance of the sparse PCE metamodels, their predictions are then compared with another testing data set comprising 613 test samples, which is totally different from the training data set. Table IV. provides the accuracy of the sparse PCE metamodels by collecting the LOO error on the training data set, the test error on the test data set, the mean values $\widehat{\boldsymbol{\mu}}_{\boldsymbol{y}}$ and the standard deviation $\widehat{\boldsymbol{\sigma}}_{\boldsymbol{y}}$.

TABLE IV. Accuracy of Sparse PCE Metamodels on Different Outputs $\boldsymbol{\mathcal{Y}}$

Sparse PCE Metamodel on Model Response $\mathcal{Y}$	LOO Error (%)	Test Error (%)	$\widehat{\mu}_y$	$\widehat{\sigma}_y$
Output power P_2 [kW]	0.13 %	0.29 %	15.3	9.1
Current amplitude ratio $\lvert A_\text{I}\rvert$	0.056 %	0.15 %	2.9	1.1
Current phase difference θ_I [degree]	2.5 %	13.7 %	87.6	3.5
Magnetic flux density leakage B_{leak} $[\mu T]$	4.1 %	7.4 %	76.4	37.5

In Table IV, it can be seen that the current phase difference θ_I and the magnetic flux density leakage B_{leak} have bigger errors than the other model responses, which means that they need more training samples to build the same accurate PCE metamodels as these of the output power P_2 and current amplitude ratio $\lvert A_\text{I}\rvert$. Of these mean values $\widehat{\boldsymbol{\mu}}_{\boldsymbol{y}}$ and standard deviations $\widehat{\boldsymbol{\sigma}}_{\boldsymbol{y}}$, the magnetic flux density leakage B_{leak} exceeds the standard defined by the ICNIRP guidelines, which will lead to a further study on the shielidng design.

Furthermore, a new data set including 1000 samples is built with inputs obtained by Monte Carlo. Then, the PDFs of the model responses obtained using both COMSOL and PCE metamodels are illustrated in Fig.5.

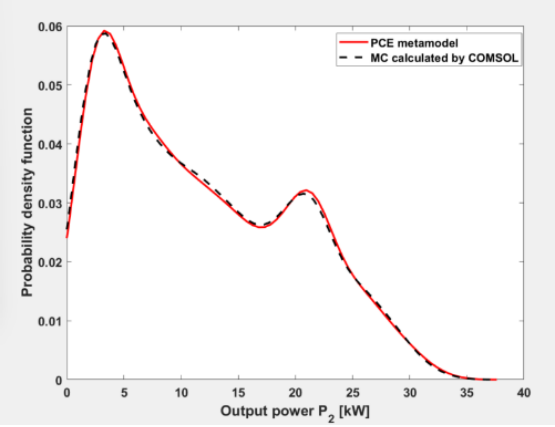

(a) PDFs of the sparse PCE metamodel for output power P_2

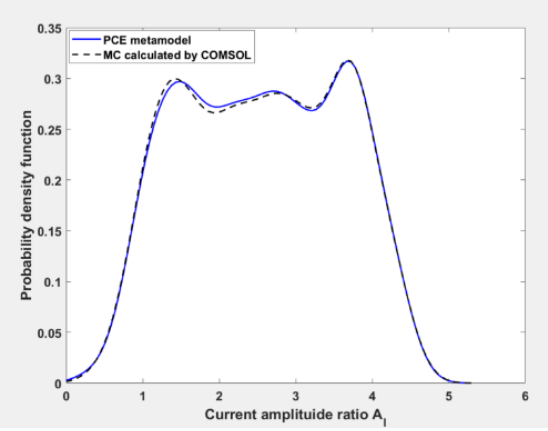

(b) PDFs of the sparse PCE metamodel for current amplitude ratio A_I

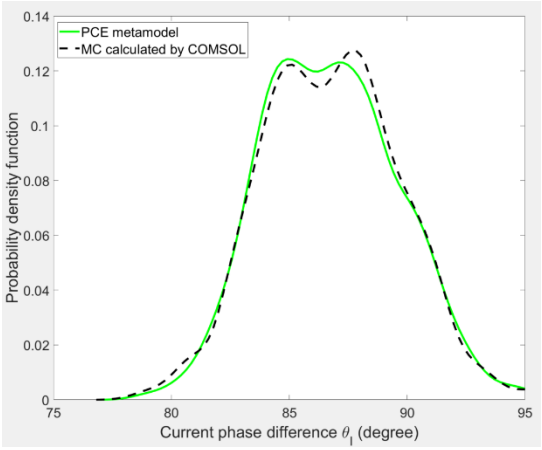

(c) PDFs of the sparse PCE metamodel for current phrase difference θ_I

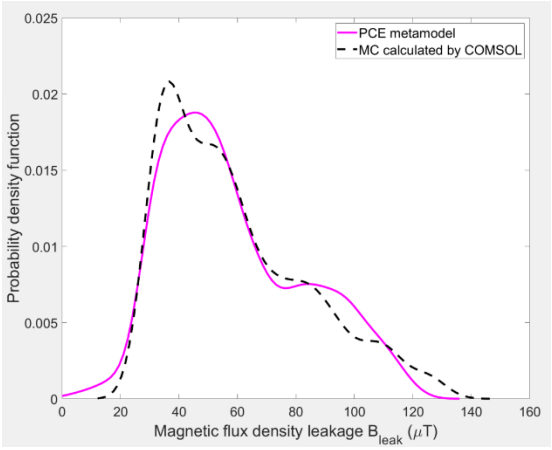

(d) PDFs of the sparse PCE metamodel for magnetic flux density leakage B_{leak}

Fig. 5. PDFs of model response $\boldsymbol{y}$ obtained from the sparse PCE metamodel

These figures shows that the PDFs estimated via PCE metamodels have a good agreement with the PDFs of Monte Carlo calculations by COMSOL. So, a sparse PCE metamodel is able to respresent the model responses $\boldsymbol{y}$ with the variability of the influencing factors, which shows that this technique may be used to choose the coil and ferrite plate sizes for the DWPT system.

Then, the values of the First-order Sobol index, calculated by Equation (9), show that how the influencing factors affect the different model responses $\boldsymbol{y}$ separately.

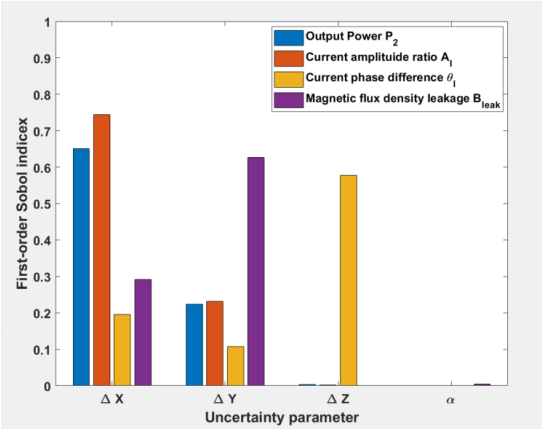

Fig. 6. First-order Sobol index for different model responses $\boldsymbol{y}$

It can be seen that the variations in the output power P_2 and the current amplitude ratio $|A_I|$ are mainly related to the moving distance along the X axis because of the reduction of magnetic field lines. The current phase difference θ_I is influenced by the vertical variation along the Z axis most. The rotation along the Z axis has almost no effect on the model responses $\boldsymbol{y}$ compared to the other factors in the given variation range. The misalignment along Y axis has the maximum impact on the magnetic flux density leakage B_{leak}, due to the reason that the observation point is on the direction of Y axis.

V. Conclusion

This work analyzes how the position of the receiver influences this realistic DWPT system based on sparse PCE metamodels. The moving distance along the X axis influences most of the output power P_2 and the current amplitude ratio $|A_I|$. However, the vertical variation along Z axis will influence the current phase difference θ_I most during the dynamic charging process, which leads to the increase of the reactive output power. The magnetic flux density leakage B_{leak} will be influenced most by the misalignment along Y axis. So it is meaningful to know the variations of the model responses with these influencing factors in order to optimize this DWPT system better. At the same time, it reveals that this metamodeling by PCE can be extended to design magnetic systems suitable for both stationary and dynamic WPT system.

References

[1] H.-Y. Mak, Y. Rong, and Z.-J. M. Shen, "Infrastructure planning for electric vehicles with battery swapping," *Manage. Sci.*, vol. 59, no. 7, pp. 1557–1575, 2013.

[2] C T. Rim, C.Mi, "Wireless Power Transfer for Electric Vehicles and Mobile Devices | IEEE eBooks | IEEE Xplore". https://ieeexplore-ieee-org.ezproxy.universite-paris-saclay.fr/book/7953908 (accessed Apr. 01, 2022).

[3] T. M. Fisher, K. B. Farley, Y. Gao, H. Bai, and Z. T. Tse, "Electric vehicle wireless charging technology: A state-of-the-art review of magnetic coupling systems," *Wireless Power Transf.*, vol. 1, no. 2, pp. 87–96, 2014.

[4] A. Mahesh, B. Chokkalingam, and L. Mihet-Popa, "Inductive Wireless Power Transfer Charging for Electric Vehicles–A Review", *IEEE Access*, vol. 9, pp. 137667–137713, 2021, doi: 10.1109/ACCESS.2021.3116678.

[5] Y. Pei, Y. Le Bihan, M. Bensetti, and L. Pichon, "Comparison of Coupling Coils for Static Inductive Power-Transfer Systems Taking into Account Sources of Uncertainty", *Sustainability*, vol. 13, no. 11, p. 6324, Jan. 2021, doi: 10.3390/su13116324.

[6] K. Kadem, M. Bensetti, Y. Le Bihan, E. Labouré, and M. Debbou, "Optimal Coupler Topology for Dynamic Wireless Power Transfer for Electric Vehicle", *Energies*, vol. 14, no. 13, p. 3983, Jan. 2021, doi: 10.3390/en14133983.

[7] V. Cirimele *et al.*, "Uncertainty Quantification for SAE J2954 Compliant Static Wireless Charge Components", *IEEE Access*, vol. 8, pp. 171489–171501, 2020, doi: 10.1109/ACCESS.2020.3025052.

[8] R. Trinchero, M. Larbi, H. M. Torun, F. G. Canavero, and M. Swaminathan, "Machine Learning and Uncertainty Quantification for Surrogate Models of Integrated Devices With a Large Number of Parameters", *IEEE Access*, vol. 7, pp. 4056–4066, 2019, doi: 10.1109/ACCESS.2018.2888903.

[9] Y. Pei, L. Pichon, M. Bensetti, and Y. Le-Bihan, "Uncertainty quantification in the design of wireless power transfer systems", *Open Physics*, vol. 18, no. 1, p. 391, Jul. 2020, doi: 10.1515/phys-2020-0174.

[10] VEDECOM. https://www.vedecom.fr/ (accessed Apr. 20, 2022).

[11] T. Imura, "Basic Circuit for Magnetic Resonance Coupling (S–S Type)", in *Wireless Power Transfer: Using Magnetic and Electric Resonance Coupling Techniques*, T. Imura, Ed. Singapore: Springer, 2020, pp. 93–111. doi: 10.1007/978-981-15-4580-1_4.

[12] K. Kadem, “Modeling and Optimization of a magnetic coupler for dynamic induction charging of electric vehicles,” Theses, Centralesupelec, 2020. Accessed: May 24, 2022. [Online]. Available: https://hal.archives-ouvertes.fr/tel-03253967.

[13] “ICNIRP Guidelines for Limiting Exposure to Electromagnetic Fields (100 kHz to 300 GHz),” *Health Physics*, vol. 118, no. 5, pp. 483–524, 2020, doi: 10.1097/HP.0000000000001210.

[14] “J2954: Wireless Power Transfer for Light-Duty Plug-in/Electric Vehicles and Alignment Methodology - SAE International.” https://www.sae.org/standards/content/j2954_202010/ (accessed Mar. 26, 2021).

[15] S. Marelli, N. Luthen, B. Sudret, “UQLab user manual – Polynomial chaos expansions”, Report UQLab-V2.0-104, *Chair of Risk, Safety and Uncertainty Quantification*, ETH Zurich, Switzerland, 2022.

[16] G. Blatman and B. Sudret, “Adaptive sparse polynomial chaos expansion based on least angle regression," *J. Comput. Phys*., vol. 230, no. 6, pp. 2345-2367, 2011.

[17] M. Larbi, H. M. Torun, M. Swaminathan, I. S. Stievano, F. G. Cañavero, and P. Besnier, “Uncertainty quantification of SiP based integrated voltage regulator," in *Proc. IEEE 22ndWorkshop Signal Power Integr*. (SPI), Brest, France, May 2018, pp. 1-4.

[18] B. Efron, T. Hastie, I. Johnstone, and R. Tibshirani, “Least angle regression”, *Ann. Statist*., vol. 32, no. 2, pp. 407-499, 2004.

[19] I. M. Sobol, “Sensitivity estimates for nonlinear mathematical models”, Math. Model. *Comput. Exp*., vol. 1, no. 4, pp. 407-414, 1990.

[20] B. Sudret, “Global sensitivity analysis using polynomial chaos expansions”, *Rel. Eng. Syst. Saf*., vol. 93, no. 7, pp. 964_979, Jul. 2008.

[21] C. Lataniotis, E. Torre, S. Marelli, B. Sudret, “UQLab user manual – The Input module”, Report UQLab-V2.0-102, *Chair of Risk, Safety and Uncertainty Quantification*, ETH Zurich, Switzerland, 2022